# Electric field enhancement and concomitant Raman spectral effects at the edges of a nanometre-thin gold mesotriangle†

P. R. Sajanlal,[a] C. Subramaniam,[a] P. Sasanpour,[b] B. Rashidian[bc] and T. Pradeep*[a]

The local electric field enhancement at various regions of an individual nanometre-thin gold mesotriangle has been demonstrated both numerically and experimentally. This work provides, for the first time, direct experimental evidence of localized enhancement of Raman signals at three edges of nanometre-thin gold mesotriangles at single particle level, using Raman microscopy. Raman images were collected from mesotriangles of ∼11 µm edge length and ∼30 nm thickness, using adsorbed crystal violet as the probe molecule. Spatial distribution and the extent of electric field enhancement around a single mesotriangle are investigated theoretically by finite-difference time-domain (FDTD) simulations. Confocal Raman studies provided direct proof for the substantial electrical field enhancement at the edges and corners compared to the face of the mesotriangle. The simulated electric field enhancement was in the order, corner > edge > surface, which is in complete agreement with the experimental results.

## Introduction

As an extremely sensitive technique enabling the detection of chemical and biochemical species at single molecule level, surface-enhanced Raman scattering (SERS)[1] has been an active area of research for the past few decades. Enhancement of the Raman signal occurs principally due to the enhancement in the electric field felt by the analyte in the vicinity of a substrate, which is often a nanomaterial. Understanding the origin of enhancement at the single particles of definite shape is of great interest since the enhancement of the electric field near it depends on its geometry. Among the anisotropic nanostructures, the nanotriangle is extensively used as a model object for theoretical studies of the electric field enhancement.[2] To study the shape-dependent SERS property of a nanoscale object, it is important to have a quantitative understanding of the electric field enhancement near the nanostructures. Our research group has been actively involved in the development of various SERS active anisotropic nanostructures.[3]

Theoretical predictions of field enhancement around various core-shell and simple nanostructures like spheres, spheroids, rods, triangles, etc. have been reported.[4] Several methods such as the multiple multipole (MMP) technique,[5] finite element,[6] boundary element,[7] and finite-difference methods have been used for the numerical calculations of electromagnetic fields generated around an object. Among them, the finite-difference time-domain (FDTD) method[8] has been used extensively because it has a distinct advantage in handling field-sample interactions.

Surface-enhanced spectroscopies are mainly based on chemical and electromagnetic interactions between the analyte molecules and metal surfaces. Electromagnetic mechanism[9] is considered to be the major factor responsible for the enhancement, which deals with the excitation of localized surface plasmons of the nanomaterials by the interaction with electromagnetic radiation, leading to the formation of 'hot spots' where the intensity of the SERS signals will be maximum.[10] Free electron resonance at the metal surface enhances the electric field. Due to the increase in the polarization of analyte molecules sitting in the vicinity of this enhanced local field, the optical cross-section enhances. This results in the increased intensity of the Raman scattered light. Since the plasma frequency of the electron gas for the metals like gold and silver lies in the optical range, this can generate a highly dispersive dielectric function at the optical frequencies[11] when these metals interact with electromagnetic radiation. For aggregated nanoparticles, a strong electric field is expected between the nanoparticles.[12]

The objective of the present work is to study the extent of SERS activity at different locations of gold mesotriangles both experimentally and theoretically. It is known that the sharp edges and tips of the metallic nanoparticles can exhibit large electromagnetic fields.[13] The resultant field will enhance the Raman vibrations of the analyte molecules at these locations. Although there have been reports on the enhanced electric field of the nanotriangles and other nanostructures using finite element, boundary element, finite difference, etc. simulation methods,[2,5,6] this is the first study which provides direct experimental and theoretical evidence for the enhanced electric field at the edges and corners compared to the faces of a single mesotriangle. However, it is to be noted that optical spectroscopies and microscopies at single particle level have been reported in several publications. We summarize these studies below. Near-field

[a] DST Unit on Nanoscience (DST UNS), Department of Chemistry and Sophisticated Analytical Instrument Facility, Indian Institute of Technology Madras, Chennai, 600 036, India. E-mail: pradeep@iitm.ac.in; Fax: +91-44 2257-0545
[b] Institute for Nano Science and Technology (INST), Sharif University of Technology, Tehran, Iran
[c] Department of Electrical and Electronic Engineering, Sharif University of Technology, Tehran, Iran

microscopic studies of surface plasmons in nanorods, triangular nanoplates, and aggregated nanospheres have been reported.[14] Using electron energy loss spectroscopy (EELS) and microscopy, the eigenmodes complementary to the optical surface plasmon polarization have been studied in Ag nanoprisms.[15] Visualization of localized intense electromagnetic fields in real space in well-tailored dimeric and trimeric gold nanospheres has also been achieved by using near-field optical technique.[10a] Surface plasmon resonance (SPR) and subsequent surface-enhanced Raman scattering of gold nanoaggregates were investigated with reference to the availability of hot sites.[16a] Electric field enhancement at a nanoscale gap between two metallic nanostructures has also been reported.[16b,c] Using interferometric homodyne tip-scattering scanning near-field optical microscopy, the selected vector field components of the local-field distribution of crystalline triangular nanoprisms have been characterized.[17] Electromagnetic mechanism of surface-enhanced Raman scattering has been probed via Au nanodisk arrays generated using on-wire lithography.[10b] Raman scattering from individual gold nanostars, coated with self-assembled monolayers of 4-mercaptobenzoic acid has also been reported.[18] Recently, we have demonstrated experimentally the enhancement of electric field at the edges of triangular gold superlattice structures, formed by the assembly of smaller spherical nanoparticles, by Raman imaging.[19]

In order to observe electric field enhancement, Raman images were collected from a single gold mesotriangle, using crystal violet (CV) as the probe molecule. Field enhancement at the edges was investigated theoretically by FDTD simulations. The dispersive behavior of permittivity has been incorporated by the Drude model.

## Experimental details

### Materials

Tetrachloroauric acid trihydrate ($HAuCl_4 \cdot 3H_2O$) and citric acid were purchased from CDH, India. CV was procured from Sigma Aldrich. All chemicals were used as such without further purification. Triply distilled water was used throughout the experiments.

### Synthesis of gold nanoplates

The gold nanoplates were synthesized through a simple citric acid reduction method. In a typical synthesis, 5 ml of 2.5 mM citric acid was taken in a sample bottle. Into this solution, 2 ml of 25 mM $HAuCl_4$ was added. The resultant solution was kept undisturbed for 50 h at room temperature. It was then centrifuged at 3000 rpm for 5 min and a sand colored residue was collected. It was washed thrice with water in order to remove unreacted ions. The residue was then redispersed in distilled water for further use. Single mesotriangles, observable under optical microscope were selected for Raman measurements.

### Methods

Scanning electron microscopic (SEM) images and energy dispersive analysis of X-ray (EDAX) studies were done in a FEI QUANTA-200 SEM. For the SEM measurements, samples were drop-cast on an indium tin oxide (ITO) conducting glass and dried. The optical, Raman and atomic force microscopy (AFM) measurements were done using a Witec GmbH confocal Raman spectrometer equipped with a 514.5 nm Ar ion laser with a maximum power of 40 mW. Several different shapes such as truncated triangles, equilateral triangles, polygons, etc. were seen in the as-synthesized plates along with a large number of triangles. They can be seen using optical microscopy, although their thicknesses are in nanometre region. For measuring Raman images, the mesotriangle-coated glass substrate was dipped in $10^{-6}$ M CV solution for 1 h. This substrate was then gently washed with distilled water, dried and mounted on a piezo-equipped scan stage of the Raman spectrometer to enable spectral imaging. The signals were then dispersed using a 600 grooves/mm grating. The back-scattered light was collected by a 100× objective at an integration time of 50 ms and sent to the spectrometer through a multimode fibre. The dispersed light was collected by a Peltier cooled charge coupled device (CCD) detector. Spectra from various parts of the Raman image were collected and analyzed. For spectral imaging, the desired area was partitioned into 15,625 squares (an imaginary 125 × 125 matrix drawn over it), with each square representing a sampling point and consequently a pixel for the image. Typical signal acquisition time at each pixel of the image was 50 ms. Intensities of the desired portion of the spectra collected over all the pixels were compared by Scan CTRL Spectroscopy Plus Version 1.32 software, to construct a color-coded image. Spectral intensities acquired over a predefined area were automatically compared to generate color-coded images. For the simulation, FDTD code has been developed in MATLAB. Code consists of implementation of 3D FDTD method in Cartesian coordinates with dispersion behaviour of permittivity. Simulations have been performed on a platform consisting of 3.0 GHz Core 2 Duo Processor of Intel with 8 GB RAM.

## Results and discussion

The characterization of mesotriangles was done by scanning electron microscopy (SEM) and atomic force microscopy (AFM). The low magnification SEM image (ESI, Fig. S1†) indicates that synthesis yields particles of hexagonal, truncated triangular and trianglular shapes along with few nearly spherical nanoparticles. Most of these plates have an edge length in the range 5–12 μm with a thickness of around 30 nm. Even though the thickness of the triangular plates is less than 100 nm, we prefer to call them mesotriangles (mesoscopic materials are characterized by a length scale ranging from 10 nm to micrometres[20]), since the edge lengths are in the range of several micrometres. These nanometre-thin mesotriangles were clearly visible under the optical microscope (ESI, Fig. S1†). Smaller particles, seen in SEM, were not observed, as expected. Fig. 1A shows an SEM image of a single gold mesotriangle synthesized by this method. The corresponding Au Mα based EDAX image (Fig. 1B) reveals the chemical composition of the mesotriangle formed. The elemental map confirmed that the triangle is principally composed of gold.

The edge length and thickness of the mesotriangle selected for the Raman study were measured by AFM. Fig. 1C shows the

This journal is © The Royal Society of Chemistry 2010

J. Mater. Chem., 2010, 20, 2108–2113 | 2109
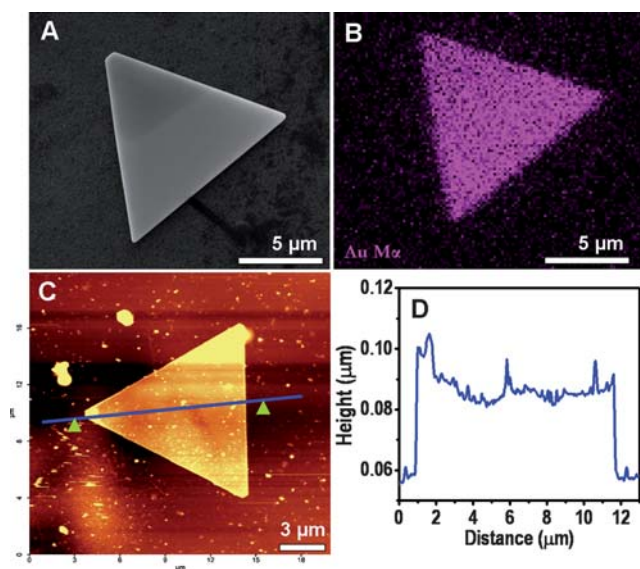
**Fig. 1** An SEM image (A) and the corresponding Au Mα based EDAX image (B) of a single nanometre-thin gold mesotriangle. (C) An AFM image of the mesotriangle used for Raman imaging. (D) A line profile taken along the diagonal of the mesotriangle, marked in C.

AFM image of the mesotriangle used for the Raman measurements. The height profile taken along the line drawn across the diagonal of the mesotriangle (marked in the image) is shown in Fig. 1D. The profile reveals that the mesotriangle has an edge length of ∼11 μm with a thickness of ∼30 nm. Line profile analysis also shows that the surface of the mesotriangle is not perfectly smooth, possibly due to the adsorbed smaller nanoparticles.

Fig. 2A shows the Raman image of a CV-adsorbed, single mesotriangle in the spectral range of 200 to 2000 cm$^{-1}$. The Raman image provides a clear picture of the geometry and the chemical environment around the mesotriangle. In the images, regions coded yellow have maximum Raman intensities and regions shown in black have minimum signal intensities. To get better clarity of the field enhancement at the edges and corners of the triangle, we selected the prominent Raman features of the adsorbed CV centered around 1100 to 1700 cm$^{-1}$ alone to generate the Raman image (Fig. 2B). Interestingly, we found a difference in the intensity of the Raman signals at various regions of the mesotriangle. Since edges of mesotriangles are highly active for electric field enhancement, a larger Raman intensity at the edges than the surface was observed. Among the three corners, the intensity of Raman signals collected from position 'b' was slightly lesser than the other two. At the same time, the Raman intensity was poor at the face of the mesotriangle. We analyzed Raman spectra collected from various points over the surface of the triangle and found that the SERS intensity varies at different locations of the surface. The roughness of the surface may be the reason for the varying SERS activity at different locations of the mesotriangle surface. It is known that highly roughened metallic surfaces can act as hot spots for Raman enhancement.

Raman images were also collected at different depths. The confocality prevents the fluorescence and the Raman signals coming from out-of-focal planes to reach the spectrometer.
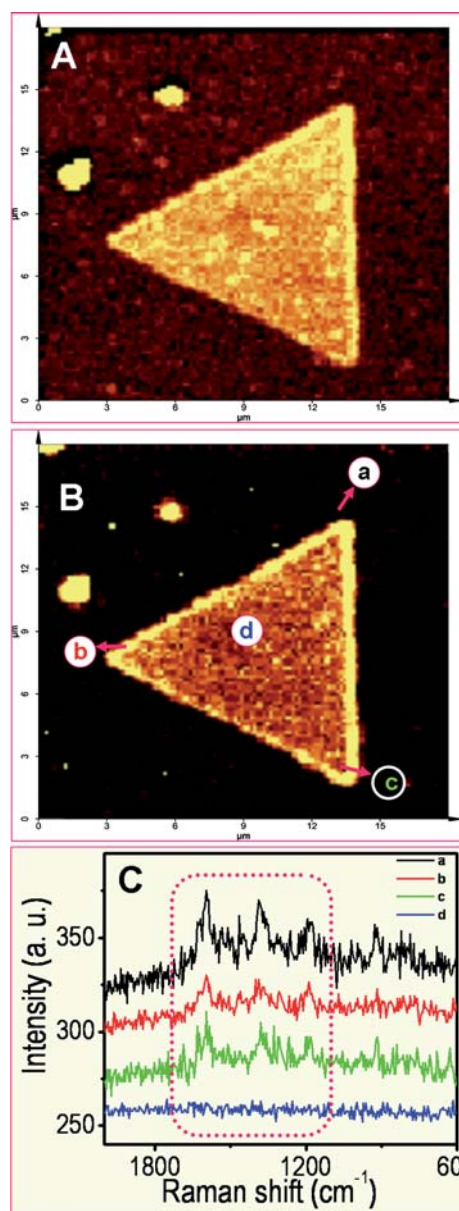


**Fig. 2** Raman images of a single mesotriangle acquired by collecting the intensities in the range of 200–2000 cm$^{-1}$ (A) and 1100–1700 cm$^{-1}$ (B). (C) Raman spectra collected from the different points marked in B. The region used for collecting image B is marked in C.

First, the microscope was positioned at the focal plane near to the surface of the mesotriangle. This was considered as the initial position. Subsequently, the microscope objective was moved downwards, in steps, towards the sample surface. Fig. 3 shows the Raman images collected this way. Each pair of images shown in Fig. 3 corresponds to the data at distinct depths ranging from 0 to 8 μm by a step of 2 μm, from the focal plane. Fig. 3A shows the images created by integrating spectral intensities in the range of 200 to 2000 cm$^{-1}$. Fig. 3B gives the data in the 1100–1700 cm$^{-1}$ window, where the Raman features of crystal violet molecules are prominent. As the objective moves closer to the sample, we observed a considerable decrease in the Raman intensities from the top surface of the mesotriangle, with the triangular frame and the edges growing in prominence.
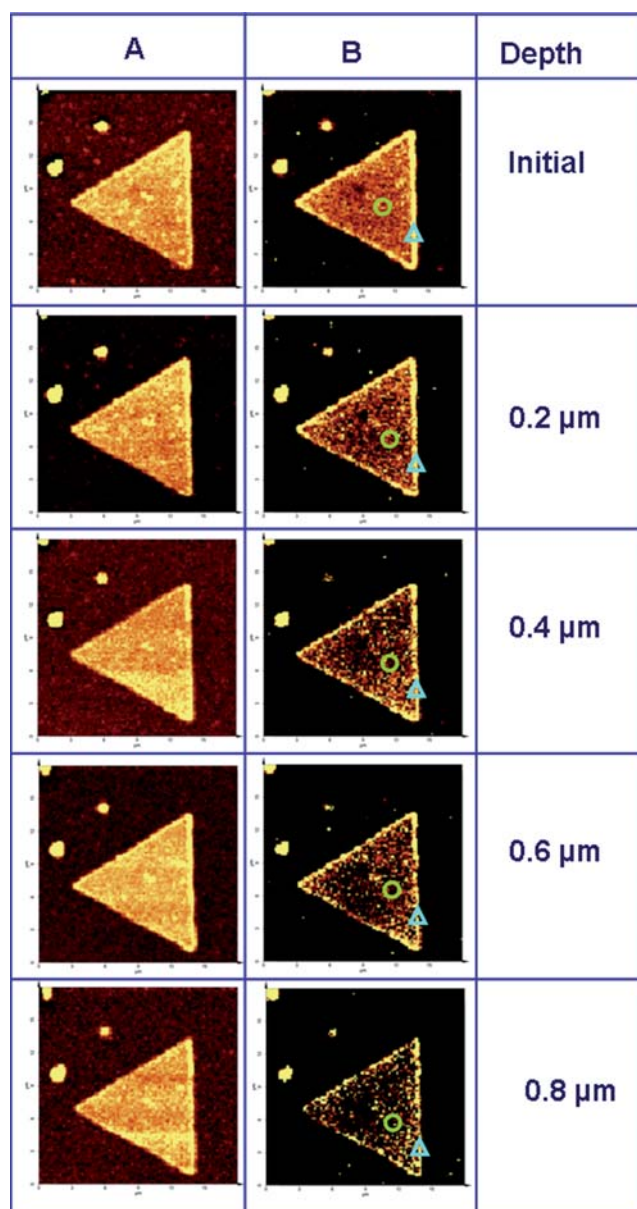
**Fig. 3** Confocal Raman images of the gold mesotriangle collected at different depths. Sets of Raman images at different depths were created by integrating Raman spectral intensities between (A) 200–2000 cm$^{-1}$ and (B) 1100–1700 cm$^{-1}$. Depths at which the images were collected are indicated. The locations from which spectra are collected are marked with circles and triangles.



**Fig. 4** Raman spectra collected from two different areas of the mesotriangle marked in Fig. 3B, at different depths. (A) From the surface and (B) from the edge. (C) A plot of intensity of the Raman band at 1595 cm$^{-1}$ verses the depth, collected from edge and the surface.

The edges dominate in all the images. We analyzed the Raman spectra collected from a specific area of the surface (marked by circles in Fig. 3B) of the mesotriangle at different depths. The spectra are presented in Fig. 4A. A decrease in the intensity of the Raman signals, as the objective moves closer to the surface of the mesotriangle was seen.

An enhancement in the Raman intensities at the edges is expected because of the increased number of analyte molecules at the edges than at the top surface in a given cross-section, as the Raman imaging is being performed normal to the surface plane. However, this possibility may be ruled out by performing the depth scan. The signal collected from the edges showed only a negligible decrease in the intensity at various depths. This indicates that the enhancement may not be due to the larger number of analyte molecules sitting at the edges, but due to the electric field generated at the edges influencing the enhancement in the Raman intensity. The Raman spectra collected from the edge of the mesotriangle (marked by triangle in the Fig. 3B) at various depths are presented in Fig. 4B. A plot of relative spectral intensity at different depth collected from the top surface and edge of the mesotriangle (positions are marked in Fig. 3B) is presented in the Fig. 4C. A drastic decrease in the intensity at the surface compared to the edge is clear in the graph. Despite this, the concentration effect cannot be completely disregarded. By optical microscopy, it will be impossible to select nanometre thin sections and so, confocal imaging alone is inadequate to judge the concentration effects. Nevertheless, the intensity enhancement is non-uniform at different edges, although concentration is expected to be uniform in view of the similar thickness. However, the presence of distinct enhancement at the edges in the images and the near-complete absence of the spectrum from the top surfaces (Fig. 2C) suggest that difference in enhancement and not concentration is the dominant factor. In order to interpret the observed results, we have simulated the local electric field enhancement around the mesotriangle using the FDTD simulation method.

## Simulation

In FDTD simulations, Maxwell's equations are discretized in time and space and differentiation operators are replaced by difference operators.[8] In order to incorporate dispersion behavior of the metal, there have been several models, of which we have used the Drude model for the simulation of field enhancement. In this, permittivity of the particle is described[11] by:

$$\varepsilon(\omega) = \varepsilon_\infty - \frac{\omega_D^2}{\omega_D^2 + i\gamma_D\omega} \qquad (1)$$

where $\varepsilon_\infty$ is the dielectric constant far above the plasmon frequency, $\omega_D$ is the plasma frequency and $\gamma_D$ is an intrinsic damping parameter. To facilitate calculation and due to the memory consuming behavior of FDTD, we have used the auxiliary differential equation (ADE) method.[8] We have used the total field scattered field (TFSF) technique in order to apply plane wave condition for the incident field, also Mur boundary condition has been used as an absorbing boundary condition (ABC).[8] We have used parameters for gold by fitting the model parameters with experimentally measured values,[21] in which $\varepsilon_\infty = 5.3983$, $\omega_D = 1.3978 \times 10^{16}$ rad/s, and $\gamma_D = 1.0334 \times 10^{16}$ rad/s.

As per the measurement, the incident light comes from the laser to the optical fiber. Light at the sample surface is randomly polarized. For better comparison between the simulation and the experiment, random polarization should be considered. In order to implement effect of random polarization, simulation has been done for two orthogonal polarizations (0° and 90° polarization of electric field). As the system of equations governing the system is linear, it can be easily shown that the result of random polarization excitation is a superposition of two orthogonal excitations:

$$\langle|E^2|\rangle = \tfrac{1}{2}\{|E_{0°}^2| + |E_{90°}^2|\} \qquad (2)$$

Incident wavelength is $\lambda_0 = 514.5$ nm. The structure which has been simulated is depicted in Fig. 5(I) and 5(II) in x-y and x-z cross sections, respectively. The simulation has been performed to get the intensities from various points marked in Fig. 5(I). Raman signals from the respective points were also analyzed to validate the simulated results. For the theoretical calculation, we have selected a gold nanotriangle with an edge length of 100 nm and height of 20 nm, which is placed on the glass substrate with refractive index, $n = 1.5$.

Fig. 5(III) and (IV) show the electric field distributions around gold layer at the vicinity of air–substrate interface for 0° and 90° polarization of electric field, respectively. The first simulation was done without a nanotriangle on the substrate, next the simulation was repeated in the presence of a nanotriangle for two polarizations. In each case, values of electric field have been normalized to that obtained from the gold free layer. Zero indices of electrical field indicate gold free simulation.

As can be seen from Fig. 5, field enhancement in 0° polarization are at points B and C and in 90°, they are at A, B and C. The results are in good agreement with the literature.[22] Experimentally obtained results are also showing the same kind of field enhancement at the edges and corners. Fig. 6(I) demonstrates temporal evolution of superposed intensities of optical field at the three corners (A, B, and C), side (D) of triangle and one point
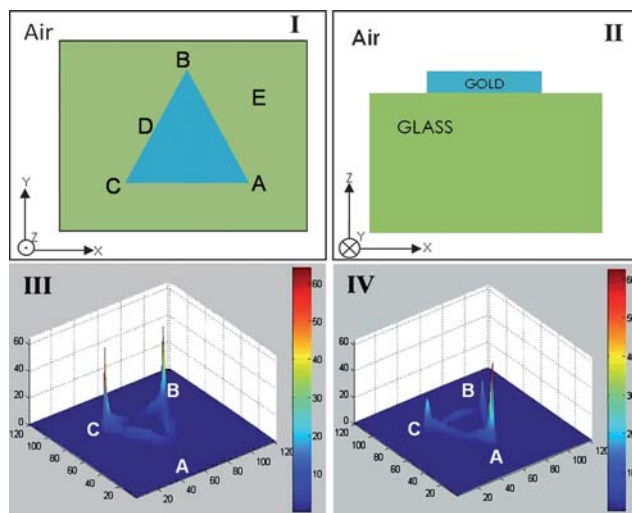


**Fig. 5** X-Y (I) and X-Z (II) cross sections of the simulated structure. Normalized electric field, $\dfrac{\sqrt{E_x^2 + E_y^2}}{\sqrt{E_{x0}^2 + E_{y0}^2}}$ distribution on the vicinity of gold layer and substrate for 0° (III) and 90° (IV) polarization of electric field.

on the glass substrate (E) for two distinct polarizations of electric field. Intensities are obtained by superposition of electric fields at two polarizations according to eqn (2).

Fig. 6(II) depicts superposed (between 0° and 90° polarization of excitation) intensity distribution *versus* distance from glass for the same points of Fig. 5(I). Zero point indicates the gold-glass contact point. According to this figure, the intensities have the highest values at the glass-gold and air-gold vicinities, respectively. From these results, it may be said that the intensities are largely enhanced at the corners and to a lower extent, at the edges. Enhancement of the intensity on the face of the nanotriangle is found to be less than at the edges and corners. The electric field is enhanced mostly at the corners. To verify the theoretical results, we analyzed the Raman spectra collected from various points from the triangle (ESI, Fig. S2†). The spectra showed an increased intensity at the corners and edges than the face of the mesotriangle. A plot of the Raman intensities (ESI, Fig. S2†) of the peak centered at 1595 cm⁻¹ collected from the mesotriangle clearly shows the difference in the field enhancement at various points. The Raman intensity was almost zero at the surface of the glass plate. The intensity was maximum at the corners of the triangle. The order of field enhancement, namely, corner > edge > surface, is in accordance with the theoretical results (ESI, Fig. S2†).

## Conclusions

In conclusion, we studied the local electric field enhancement at the various regions of isolated gold mesotriangles, both experimentally and numerically. Confocal Raman studies showed a substantial enhancement in the electrical field at the edges and corners compared to the face of the mesotriangle. We have performed FDTD simulations to find the spatial distribution and the extent of electric field enhancement around a single nanotriangle. Simulations have been done for two orthogonal
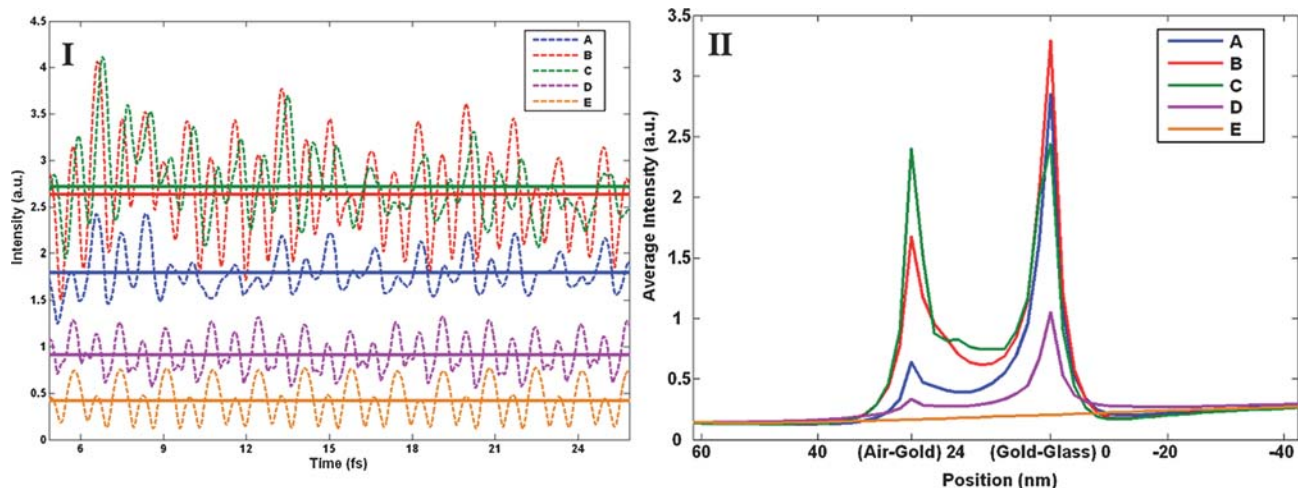
**Fig. 6** (I) Temporal evolution of superposed (between 0° and 90° polarization of excitation) intensities in the vicinity of substrate and the gold nanotriangle. Solid lines indicate the mean value (A, B, C, D, and E are same points indicated in Fig. 5(I)). (II) Superposed (between 0° and 90° polarization of excitation) intensity distribution *versus* distance (A, B, C, D, and E are the same points indicated in Fig. 5(I)). Zero points indicate gold-glass contact point.

polarizations (0° and 90°) and the results are in good agreement with the experiments. The electric field enhancement was in the order corner > edge > surface. Though there are plenty of theoretical predictions on the filed enhancement around triangular nanoparticles, we provide theoretical results and experimental evidence simultaneously for the first time by performing FDTD simulations and single particle Raman imaging.

## References

1 (a) M. Moskovits, *Rev. Mod. Phys.*, 1985, **57**, 783–826; (b) K. Kneipp, H. Kneipp, I. Itzkan, R. R. Dasari and M. S. Feld, *J. Phys.: Condens. Matter*, 2002, **14**, R597–R624; (c) G. C. Schatz, *Acc. Chem. Res.*, 1984, **17**, 370–376.
2 (a) M. J. R. Previte, K. Aslan and C. D. Geddes, *Anal. Chem.*, 2007, **79**, 7042–7052; (b) J. P. Kottmann, O. J. F. Martin, R. S. David and S. Sheldon, *New J. Phys.*, 2000, **2**, 27.
3 (a) P. R. Sajanlal and T. Pradeep, *Nano Res.*, 2009, **2**, 306–320; (b) P. R. Sajanlal and T. Pradeep, *Adv. Mater.*, 2008, **20**, 980–983; (c) P. R. Sajanlal and T. Pradeep, *Adv. Mater.*, 2009, **21**, 1320–1321; (d) P. R. Sajanlal and T. Pradeep, *Langmuir*, 2010, **26**, 456–465; (e) Ammu Mathew, P. R. Sajanlal and T. Pradeep, *J. Cryst. Growth*, 2009, DOI: 10.1016/j.jcrysgro.2009.11.039.
4 (a) M. Futamata, Y. Maruyama and M. Ishikawa, *J. Phys. Chem. B*, 2003, **107**, 7607–7617; (b) K. L. Kelly, E. Coronado, L. L. Zhao and G. C. Schatz, *J. Phys. Chem. B*, 2003, **107**, 668–677; (c) D. P. Fromm, A. Sundaramurthy, P. J. Schuck, G. Kino and W. E. Moerner, *Nano Lett.*, 2004, **4**, 957–961; (d) Z.-Q. Tian, B. Ren, J.-F. Li and Zhi-Lin Yang, *Chem. Commun.*, 2007, 3514–3534; (e) P.-P. Fang, J.-F. Li, Z.-L. Yang, L.-M. Li, B. Ren and Z.-Q. Tian, *J. Raman Spectrosc.*, 2008, **39**, 1679–1687; (f) H. Jiang, J. Sabarinathan, T. Manifar and S. Mittler, *J. Lightwave Technol.*, 2009, **27**, 2264–2270.
5 C. Hafner, *The Generalized Multiple Multipole Technique for Computational Electromagnetics*, Artech, Boston, 1990.
6 (a) J. P. Kottmann and O. J. F. Martin, *Opt. Express*, 2001, **8**, 655–663; (b) J. P. Kottmann and O. J. F. Martin, *IEEE Trans. Antennas Propag.*, 2000, **48**, 1719–1726.
7 (a) J. Aizpurua, G. W. Bryant, L. J. Richter and F. J. Garcia de Abajo, *Phys. Rev. B: Condens. Matter Mater. Phys.*, 2005, **71**, 235420; (b) K. -H. Su, Q.-H. Wei, X. Zhang, J. J. Mock, D. R. Smith and S. Schultz, *Nano Lett.*, 2003, **3**, 1087–1090.
8 (a) A. Taflove and S. C. Hagness, *Computational Electrodynamics: The Finite-Difference Time Domain Method*, Artech House, 3rd edn, 2005; (b) F. Hao, C. L. Nehl, J. H. Hafner and P. Nordlander, *Nano Lett.*, 2007, **7**, 729–732.
9 (a) H. Xu, J. Aizpurua, M. Kall and P. Apell, *Phys. Rev. E: Stat. Phys., Plasmas, Fluids, Relat. Interdiscip. Top.*, 2000, **62**, 4318–4324; (b) J. Gersten and A. Nitzan, *J. Chem. Phys.*, 1980, **73**, 3023–3037.
10 (a) K. Imura, H. Okamoto, M. K. Hossain and M. Kitajima, *Nano Lett.*, 2006, **6**, 2173–2176; (b) L. Qin, S. Zou, C. Xue, A. Atkinson, G. C. Schatz and C. A. Mirkin, *Proc. Natl. Acad. Sci. U. S. A.*, 2006, **103**, 13300–13303.
11 C. F. Bohren and D. R. Huffman, *Absorption and Scattering of Light by Small Particles*; Wiley: New York, 1983.
12 P. Muhlschlegel, H,-J. Eisler, O. J. F. Martin, B. Hecht and D. W. Pohl, *Science*, 2005, **308**, 1607–1609.
13 (a) J. T. Krugg II, E. S. Sánchez and X. S. Xie, *J. Chem. Phys.*, 2002, **116**, 10895–10901; (b) P. S. Kumar, I. Pastoriza-Santos, B. Rodríguez-González, F. J. Garcia de Abajo and L. M. Liz-Marzán, *Nanotechnology*, 2008, **19**, 15606.
14 (a) H. Okamoto and K. Imura, *J. Mater. Chem.*, 2006, **16**, 3920–3928; (b) H. J. Maas, J. Heimel, H. Fuchs, U. C. Fischer, J. C. Weeber and A. Dereux, *J. Microscopy*, 2003, **209**, 241–248.
15 J. Nelayah, M. Kociak, O. Stephan, F. J. Garcia de Abajo, M. Tence, L. Henrard, D. Taverna, I. Pastoriza-Santos, L. M. Liz-Marzan and C. Colliex, *Nat. Phys.*, 2007, **3**, 348–353.
16 (a) M. K. Hossain, G. G. Huang, T. Kaneko and Y. Ozaki, *Chem. Phys. Lett.*, 2009, **477**, 130–134; (b) A. Dhawan, S. J. Norton, M. D. Gerhold and T. Vo-Dinh, *Opt. Express*, 2009, **17**, 9688–9703; (c) M. Futamata, Y. Maruyama and M. Ishikawa, *J. Mol. Struct.*, 2005, **735–736**, 75–84.
17 M. Rang, A. C. Jones, F. Zhou, Z. -Y. Li, B. J. Wiley, Y. Xia and M. B. Raschke, *Nano Lett.*, 2008, **8**, 3357.
18 C. Hrelescu, T. K. Sau, A. L. Rogach, F. Jäckel and J. Feldmann, *Appl. Phys. Lett.*, 2009, **94**, 153113.
19 E. S. Shibu, K. Kimura and T. Pradeep, *Chem. Mater.*, 2009, **21**, 3773–3781.
20 (a) Z.-L. Xiao, C. Y. Han, W.-K. Kwok, H.-H. Wang, U. Welp, J. Wang and G. W. Crabtree, *J. Am. Chem. Soc.*, 2004, **126**, 2316–2317; (b) R. M. Penner, *J. Phys. Chem. B*, 2002, **106**, 3339–3353.
21 P. B. Johnson and R. W. Christy, *Phys. Rev. B: Solid State*, 1972, **6**, 4370–4379.
22 E. Hao and G. C. Schatz, *J. Chem. Phys.*, 2004, **120**, 357–366.

This journal is © The Royal Society of Chemistry 2010

*J. Mater. Chem.*, 2010, **20**, 2108–2113 | 2113